

Supplementary Information

Pushing CO₂-philic Membrane Performance to the limit by Designing Semi-Interpenetrating Networks for Sustainable CO₂ Separations

*Xu Jiang, Songwei Li and Lu shao**

MIIT Key Laboratory of Critical Materials Technology for New Energy Conversion and Storage, State Key Laboratory of Urban Water Resource and Environment (SKLUWRE), School of Chemistry and Chemical Engineering, Harbin Institute of Technology, Harbin 150001, PR China. E-mail: shaolu@hit.edu.cn

ESI contents

Fig. S1 Schematic of home-made UV lamb box

Fig. S2 Schematic diagram of dense membrane gas permeation testing apparatus

Fig. S3 Schematic diagram of the PALS system

Fig. S4 Chemical structures of PEGs and cross-linked networks

Fig. S5 Digital images of SIPN membranes

Fig. S6 AFM images and surface roughness of SIPN membranes

Fig. S7 SEM images of SIPN membranes

Fig. S8 TGA and DTG results of SIPN membranes

Fig. S9 XRD patterns of SIPN membranes

Fig. S10 DSC curves of SIPN membranes

Fig. S11 Density data of SIPN membranes

Fig. S12 Gas permeability, selectivity, CO₂ diffusivity and solubility of SIPN-X-Y-10 membranes.

Table. S1 o-Ps lifetimes, intensities calculated from PATFIT Program

Table. S2 Calculated *d*-spaces of amorphous SIPN-7-3-Z membranes

Table. S3 Calculated *d*-spaces of amorphous SIPN-X-Y-10 membranes

Table. S4 Gas permeability and selectivity of SIPN-X-Y-10 membranes

Table. S5. Gas permeability and selectivity of SIPN-7-3-Z membranes

Table. S6 CO₂ diffusivity, solubility and selectivity over N₂ for SIPN-7-3-Z

Table. S7 CO₂ diffusivity, solubility and selectivity over N₂ for SIPN-X-Y-10

1. Materials and instruments

1.1. Materials

Poly (ethylene glycol) methyl ether acrylate (PEGMEA, average $M_w=480$, contains 100 ppm 2,6-Di-tert-butyl-4-methylphenol (BHT) as inhibitor, 100 ppm 4-Methoxyphenol (MEHQ) as inhibitor). Poly (ethylene glycol) diacrylate (PEGDA, average $M_w=700$), 1-Hydroxycyclohexyl Phenyl Ketone (HCPK, 99%), Poly (ethylene glycol) dimethyl ether (PEGDME, average $M_w=500$, contains 100 ppm BHT as stabilizer) purchased from Sigma-Aldrich and used as received.

1.2 Instrument

XRD

X-Ray diffraction (XRD) measurements were carried on a Bruker D8 ADVANCE X-ray diffractometer at 40 kV and 40 mA for Cu $K\alpha$ ($\lambda=1.5418 \text{ \AA}$) with a scan speed of $5^\circ/\text{min}$ and a scan range from 5° to 80° .

d -space is calculated by Bragg's equation:

$$d = \frac{\lambda}{2\sin\theta} \quad (1)$$

Where λ is the wavelength of Cu $K\alpha$ radiation (1.5418 \AA), and θ is the angle of the reflection peak.

ATR-FTIR

Attenuated total reflectance Fourier transform infrared (ATR-FTIR) spectra ($4000\text{-}500 \text{ cm}^{-1}$) were collected in the solid state on a Spectrum One FT-IR spectrometer.

XPS

X-ray photoelectron spectroscopy (XPS) were collected on a PHI5700 ESCA system X-ray photoelectron spectrometer with an excitation source as $AlK\alpha$ and a working voltage at 30V under a vacuum of 10^{-6} Pa .

DSC

The differential scanning calorimeter (DSC) was performed on a DSC-Q2000 (TA, USA) from -100° C to 200° C with a heating rate of $10^\circ \text{ C}/\text{min}$ under dry N_2 purge ($50 \text{ mL}/\text{min}$).

Density test

The densities of the membranes were measured with a FA2104J 210 g/0.1 mg electronic density balance. Each sample were measured for 5 times and averaged.

NMR

The cross-linked structure of SIPN membranes was further characterized by solid-state ^{13}C Nuclear Magnetic Resonance (NMR) (100.6 MHz) with magic angle spinning (MAS) at 7.5 kHz performed on a Bruker AV 400 WB spectrometer.

TGA

Thermal gravimetric analysis (TGA) was characterized in the temperature range from room temperature to 700 °C under N_2 atmosphere and a heating rate of 10 °C/min using a PerkinElmer TGA400 analyzer.

AFM

Surface roughness test were carried on an Atomic force microscope (Broker, Dimension fast) u with a 2×2 um scan area

SEM

The morphologies of the SIPNs were observed by a scanning electron microscope (Hitachi S-4500, Japan)

2. Preparation of SIPN membranes

PEGMEA, PEGDA and PEGDME with different mass ratio were firstly homogeneously mixed with 0.1 wt% photoinitiator HCPK by sufficient stirring. The PEO mixture was then sandwiched between two quartz plates and put in the middle of UV lamp box and the solid membranes formed after 90 s UV irradiation. The fabrication was carried in a home-made UV lamp box consisting of 4×8 W medium wave UV lamps fixed on the ceiling. The above operations were conducted under room temperature (25 °C) and atmosphere.

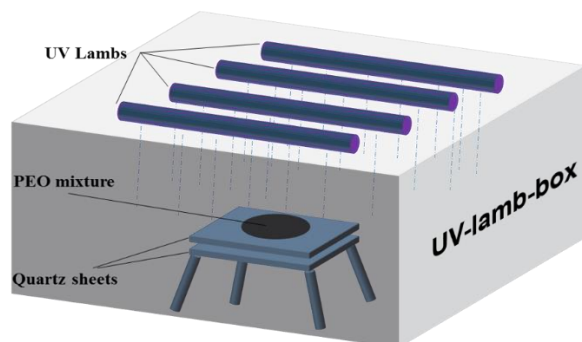


Fig. S1 Schematic of home-made UV lamp box. The wavelength of the lamps is 308 nm and the power is 4×8 W.

3. Gas permeation tests

The gas transport properties of dense membranes can be explained by the solution-diffusion mechanism. It is assumed that the Fick's law is obeyed and upstream pressure is much higher than the downstream pressure. The pure gas permeability (P) with the unit of Barrer (1 Barrer= 10^{-10} cm³(STP) cm/ (cm² s cm Hg) can be given by:

$$P = D \times S \quad (2)$$

Where D is the average effective diffusivity with the unit of cm²/s and S is the apparent sorption coefficient with the unit of cm³ (STP) /cm³ cm Hg. The ideal selectivity of a membrane for gas A over gas B is defined as the ratio of their pure gas permeabilities:

$$\alpha_{\frac{A}{B}} = \frac{P_A}{P_B} = \left[\frac{D_A}{D_B} \right] \times \left[\frac{S_A}{S_B} \right] \quad (3)$$

In this study, pure gas permeabilities was performed with a constant volume method.¹ The gases were test in the sequence of H₂, N₂, CH₄ and CO₂ at 3.5 atm and 35 °C. The gas permeability (P) was computed from the steady increase rate of downstream-pressure (dp/dt) with following equation:

$$P = \frac{273 \times 10^{10}}{760} \frac{Vl}{AT \left(p_2 \times \frac{76}{14.7} \right)} \frac{d_p}{d_t} \quad (4)$$

where V is the volume of the downstream chamber (cm³), l is the membrane thickness (cm). A refers to the effective test area of the membrane (cm²), T is the operating temperature (K) and p_2 is the upstream operating pressure (psi). The diffusivity can be calculated by the time-lag method as Equation 5 expressed, and then the solubility can be simply deduced according to Equation 2²

$$D = \frac{l^2}{6\theta} \quad (5)$$

where θ is the diffusion time lag extrapolated from the plot of pressure with time at steady state to the time axis.

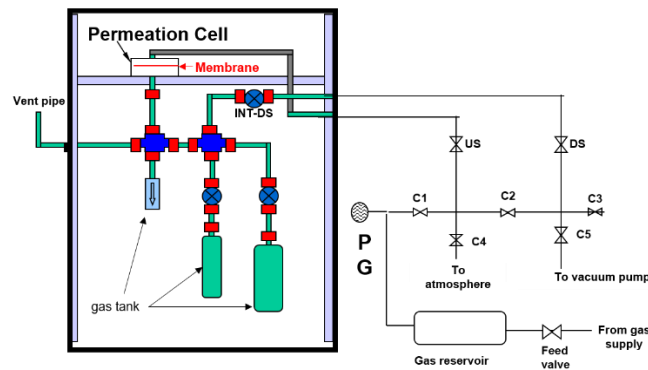


Fig. S2 Schematic diagram of dense membrane gas permeation testing apparatus

4. Mixed gas tests

Mixed gas permeation properties of SIPN membrane were investigated based on a binary 50% CO₂ and 50% N₂ mixture under 35 °C. To ensure constant gas molarity in the retentate, small amounts of retentate are slowly discharged into water or the atmosphere via a silicon piping. The sampling process was initiated by evacuating the line from the receiving volume (the lower chamber: downstream) to GC by vacuum pump. The compositions of the feed and permeate were analyzed by GC. The choice of carrier gas in the GC setup is nitrogen. Detailed experimental and set-up descriptions can also be found elsewhere^{3,4}. Permeability of each gas can be determined using the following equations:

$$P_A = \frac{273 \times 10^{10}}{760} \frac{y_A \times V \times l}{AT(P_2 \times \phi_A \times (76/14.7) \times x_A)} \frac{dp}{dt} \quad (6)$$

$$P_B = \frac{273 \times 10^{10}}{760} \frac{y_B \times V \times l}{AT(P_2 \times \phi_B \times (76/14.7) \times x_B)} \frac{dp}{dt} \quad (7)$$

where P_A and P_B refer to the permeability of CO₂ and N₂ respectively. P_2 symbolizes the upstream feed gas pressure (psi). x and y represent molar fractions of the gas in feed and permeate sides, respectively. ϕ_A , ϕ_B indicate fugacity coefficients of respective gases in the upstream.

The mixed gas selectivity is expressed by the following equation:

$$\alpha_{\frac{A}{B}} = \frac{P_A}{P_B} \quad (8)$$

5. PALS tests

The free volume size and distribution of the SIPN membranes were probed by positron annihilation lifetime spectroscopy (PALS). A fast-fast coincident PALS spectrometer in our laboratory with a system channel width of 50.53 picoseconds per channel was used to measure the lifetime and intensity of positron species. Figure S3 illustrates the schematic diagram of the bulk PALS system and a detailed description of the experimental process can be found elsewhere.^{5,6} A ^{22}Na isotope sealed in Kapton film was used as positron and γ -ray (1274 KeV) sources. Membrane samples were cut into pieces with a dimension of 1×1 cm. The sealed source was sandwiched in between two stacks of membrane samples of about 0.5 mm thick at each side. All the measurements were performed at a counting rate of approximately 200 cps and the total number of counts for each spectrum was 1.0 million. The PALS spectra were analyzed by PATFIT program. The influence of the Kapton film was excluded during the fitting by applying a pre-calibrated source correction intensity of 15% with a lifetime of 0.38 ns.

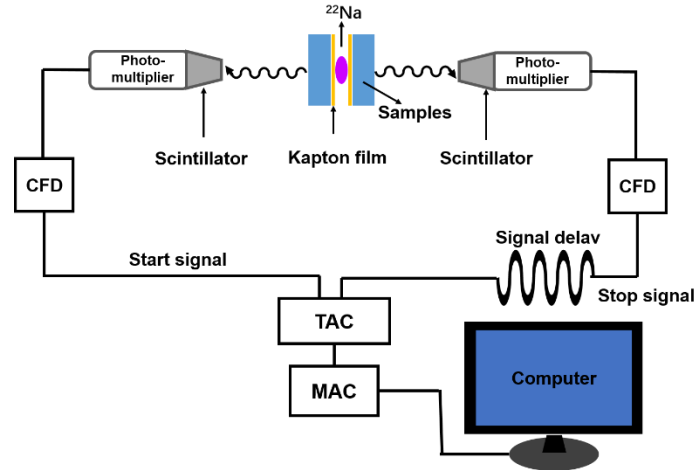


Fig. S3 Schematic diagram of the PALS system (CFD: Constant fraction discriminator; TAC: Time to amplitude converter; MCA: Multi channel analyzer).

Para-positronium (p -Ps) lifetime, τ_1 , was fixed to 0.125 ns. Free positron lifetime, τ_2 , and two orthopositronium (o -Ps) lifetimes, τ_3 and τ_4 , with their respective intensity, I_3 and I_4 were simulated. The o -Ps lifetimes, derived from the so-called pick-off annihilation with electrons in molecules, were commonly associated with the mean radii R_n (Å to nm) of the free volume elements based on a semiempirical correlation equation derived from a spherical-cavity model⁷⁻⁹:

$$\tau_n = \frac{1}{2} \left[1 + \frac{R_n}{R_0} + \frac{1}{2\pi} \sin\left(\frac{2\pi R_n}{R_0}\right) \right]^{-1} \quad (9)$$

where n is 3 or 4 while R_0 is the infinite spherical potential radius that is equal to $R_n + \Delta R$ with ΔR as a homogeneous electron layer in the infinite potential barrier ($=1.66$ Å). The relative fractional free volume (FFV) is calculated based on the Williams–Landel–Ferry (WLF) equation¹:

$$FFV = \sum_n 0.0018 I_n \left(\frac{4}{3} \pi R_n^3 \right) \quad (10)$$

where n is 3 or 4 and I is the lifetime intensity. FFV derived from τ_3 and I_3 is referred as FFV₃ and FFV derived from τ_4 and I_4 as FFV₄. The fitting results are as listed in Table S1.

Table. S1 o-Ps lifetimes, intensities calculated from PATFIT Program with a four-lifetime model

Sample	τ_3 (ns)	$\Delta\tau_3$ (ns)	τ_4 (ns)	$\Delta\tau_4$ (ns)	I_3 (%)	ΔI_3 (%)	I_4 (%)	ΔI_4 (%)	Variance
SIPN-7-3-0	0.7302	0.1481	2.5132	0.0248	7.4523	3.2747	18.8812	0.3889	1.0160
SIPN-7-3-5	0.7319	0.1383	2.5327	0.0249	7.5882	3.0297	18.5391	0.3757	1.0350
SIPN-7-3-10	0.9781	0.1631	2.5900	0.0386	5.9678	0.8013	17.5124	0.6630	1.0780

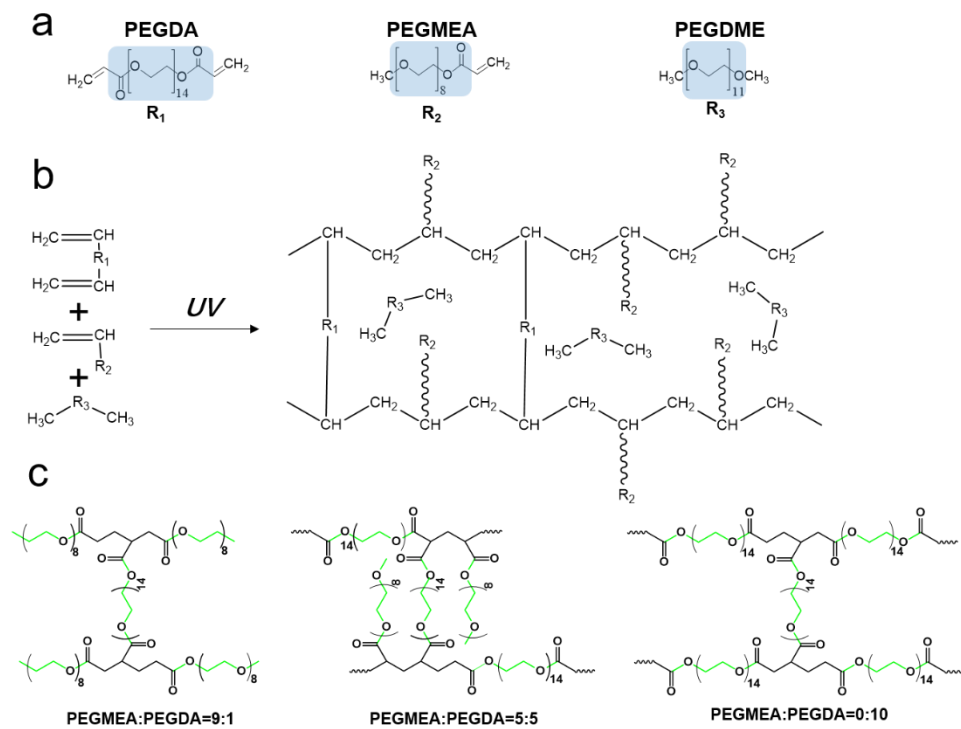


Fig. S4 (a) Chemical structure of PEG monomers and PEGDME. (b) Synthetic route outline, ideal chemical structure of SIPN membrane. (c) Schematic illustration of crosslinking network structures with different PEGMEA/PEGDA ratio.

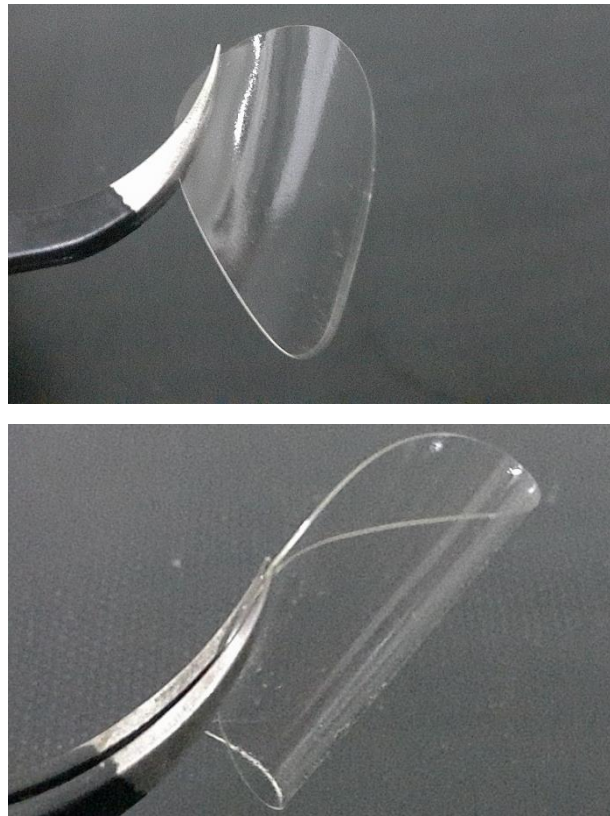


Fig. S5 Digital images of transparent and flexible SIPN-7-3-10.

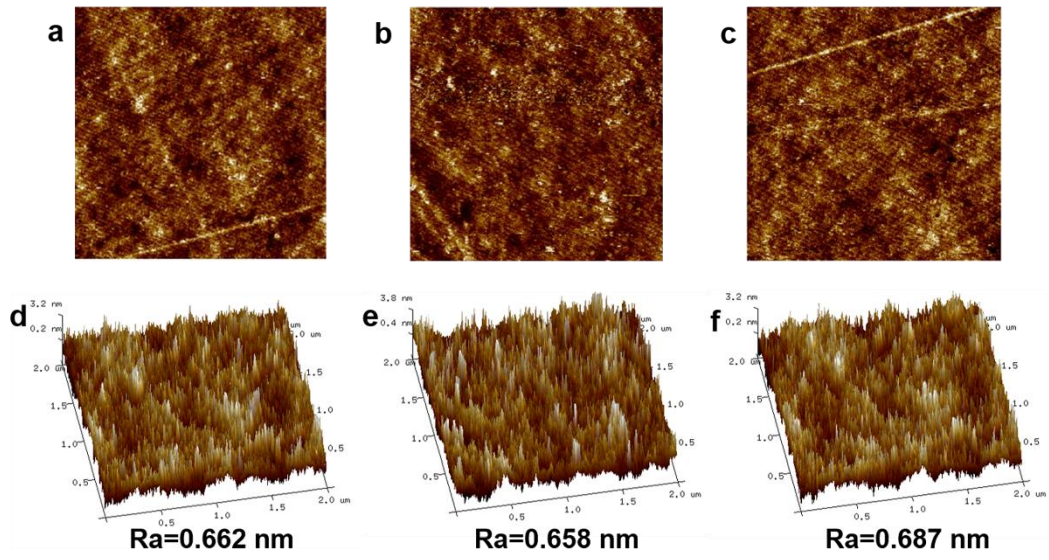


Fig. S6 AFM images and surface roughness of (a)(d) SIPN-7-3-0, (b)(e) SIPN-7-3-5 and (c)(f) SIPN-7-3-10

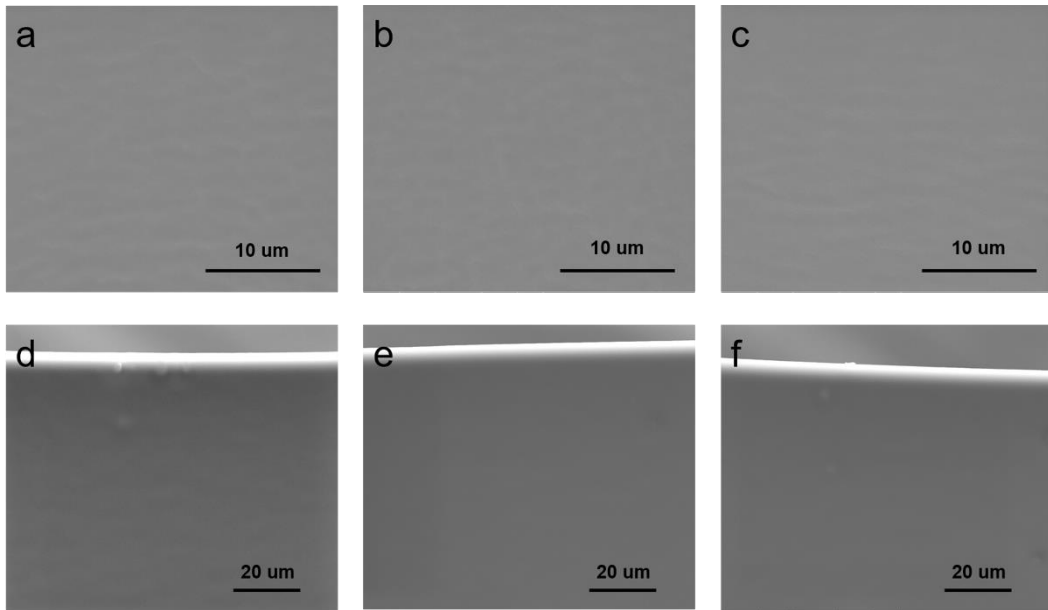


Fig.S7 SEM images of SIPN-7-3-0 (a) surface and (d) cross-section, SIPN-7-3-5(b) surface and (e) cross-section, SIPN-7-3-10(c) surface and (f) cross-section

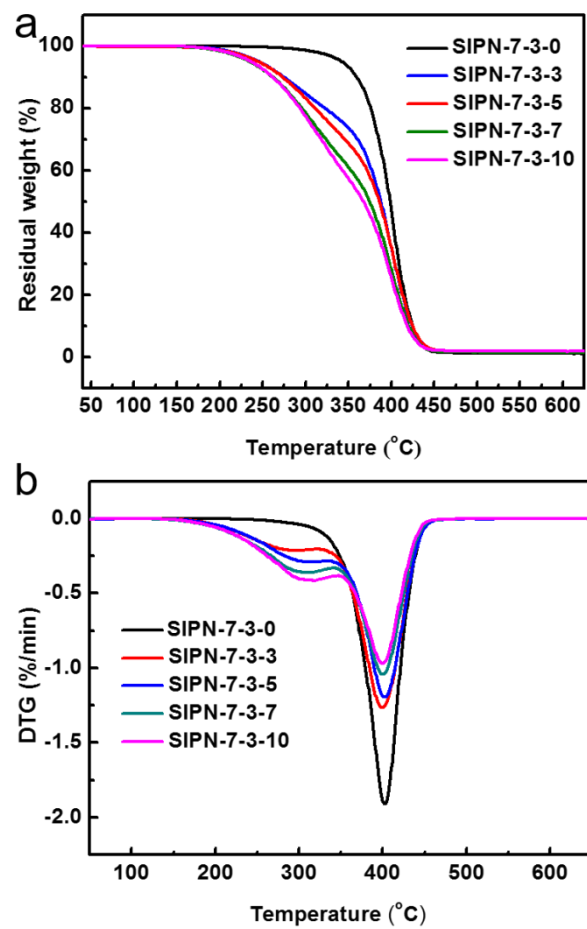


Fig. S8 (a) TGA and (b) DTG of SIPN-7-3-Z

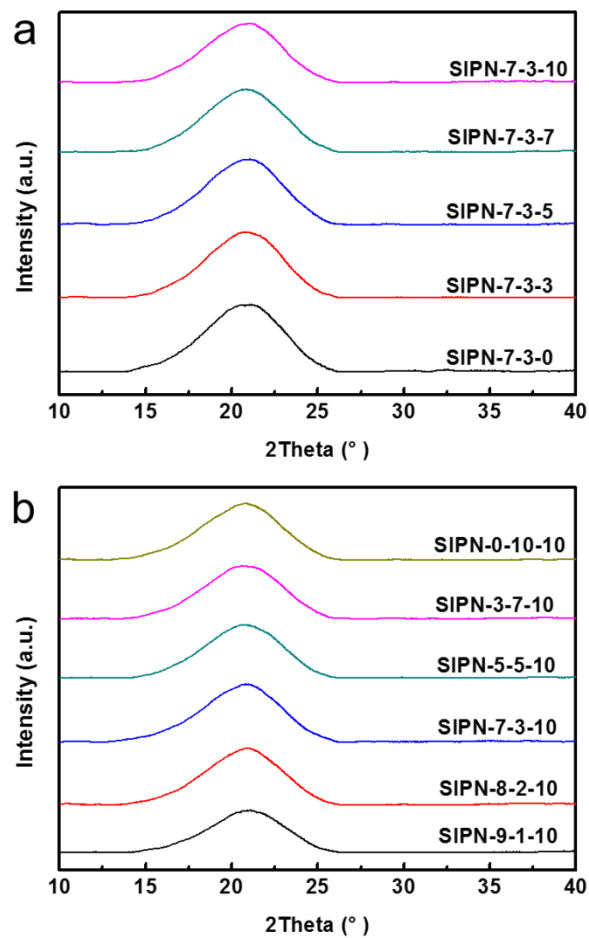


Fig. S9 XRD patterns of (a)SIPN-7-3-Z (b)SIPN-X-Y-10

Table. S2 *d*-space of amorphous SIPN-7-3-Z membranes

Membrane	<i>d</i> -space (Å)
SIPN-7-3-0	4.195
SIPN-7-3-3	4.203
SIPN-7-3-5	4.205
SIPN-7-3-7	4.225
SIPN-7-3-10	4.224

Table. S3 *d*-space of amorphous SIPN-X-Y-10 membranes

Membrane	<i>d</i> -space (Å)
SIPN-0-10-10	4.232
SIPN-3-7-10	4.240
SIPN-5-5-10	4.237
SIPN-7-3-10	4.224
SIPN-8-2-10	4.218
SIPN-9-1-10	4.217

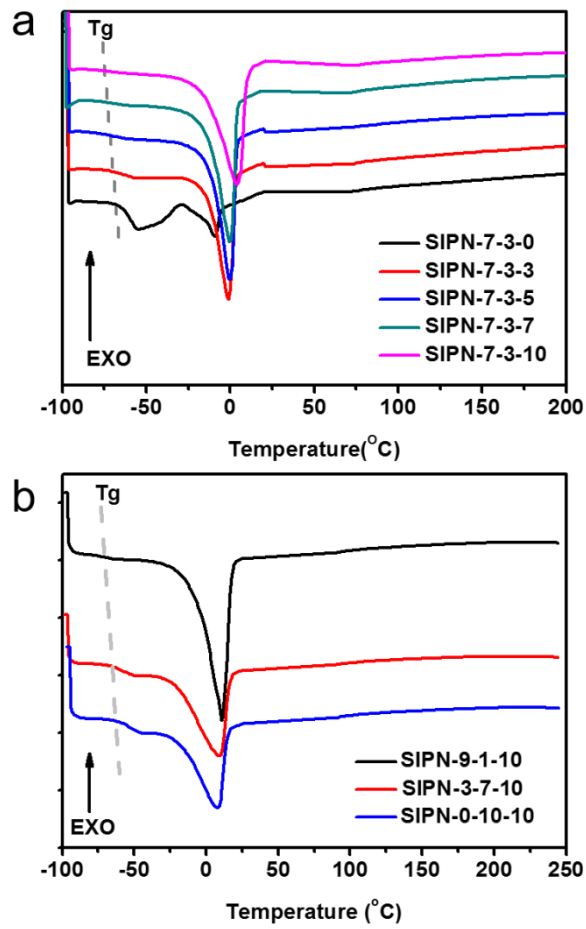


Fig. S10 DSC curves of (a) SIPN-7-3-Z and (b) SIPN-X-Y-10 membranes.

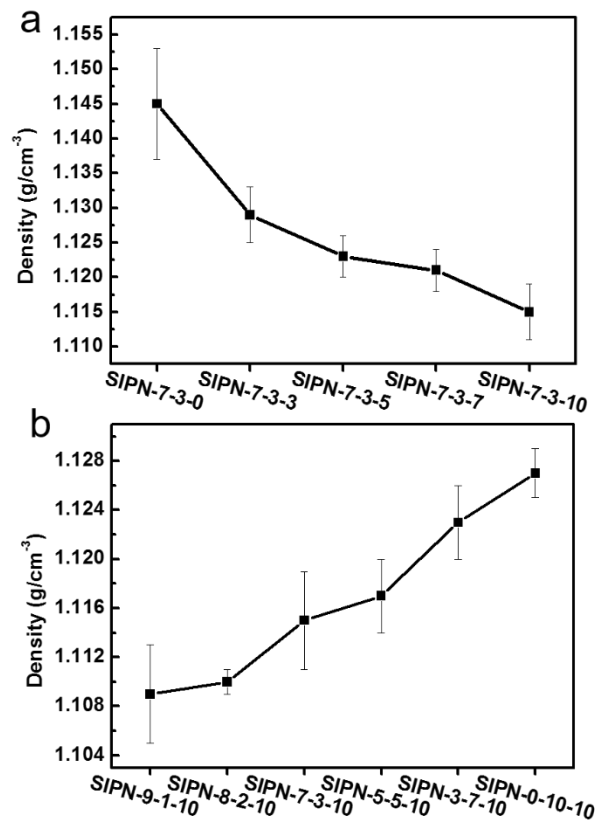


Fig. S11 Density data of SIPN membranes.

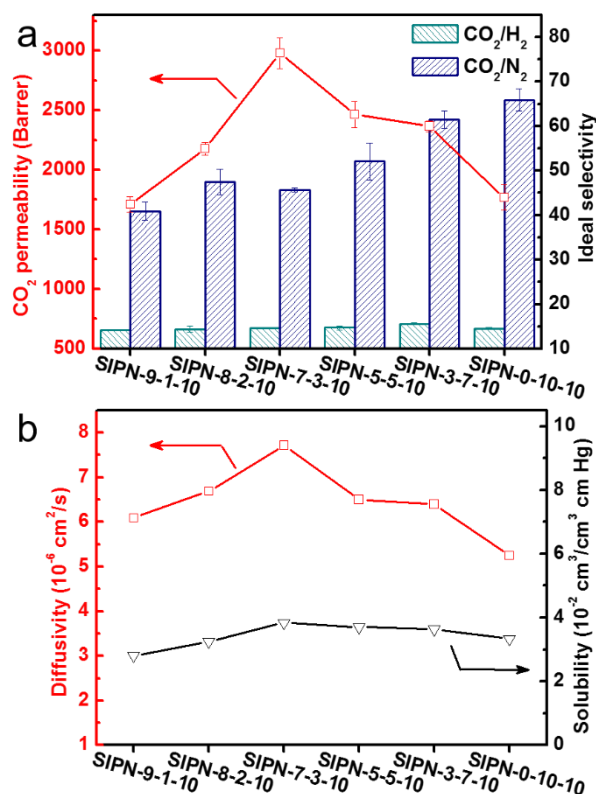


Fig. S12 (a) Gas permeability and selectivity of SIPN-X-Y-10 membranes. (b) CO₂ diffusivity and solubility of SIPN-X-Y-10 membranes.

As shown in Fig. S12(a), CO₂ permeability firstly increased with PEGDA content and reached highest value when PEGMEA/PEGDA ratio is 7/3, but then decreased at higher PEGDA content, which is in accord with the variation of diffusivity (Fig. S12(b)). Meanwhile, CO₂ solubility was slightly changed and its influence could be neglected. To determine the effect of membrane structure with different crosslinking density, we calculated the *d*-space of each membrane according to the XRD patterns using Bragg's equation and the results are shown in Table. S3. The *d*-space ascended with PEGDA content because PEGDA possesses longer molecular chain than PEGMEA and PEGDME and will stretch the cross-linked backbone, leading to an increase of gas diffusivity as well as permeability at low crosslinking density. Additionally, the cross-linked backbone became stiffer as the PEGDA monomer further increased, which is manifested in T_g rise (Fig. S10(b)), resulting in descents of gas diffusivity and permeability when PEGMEA/PEGDA ratio is below 7/3. The depressed chain mobility and diffusivity decay frustrated the permeability of larger N₂ molecule more than CO₂ molecule, contributing to 45% increase in CO₂/N₂ selectivity (45.7 to 65.9). When PEGMEA/PEGDA ratio is 7:3, the best CO₂ permeability of SIPN membrane with good selectivity can be obtained from the reasonable cross-linking density, membrane-CO₂ attraction and chain flexibility.

Table. S4 Gas permeability and selectivity of SIPN-X-Y-10 membranes

Membrane	PEGMEA:PEGDA:PEGDME	Permeability (Barrer)			Ideal Selectivity	
		H ₂	N ₂	CO ₂	CO ₂ /H ₂	CO ₂ /N ₂
SIPN-9-1-10	9:1:10	120.7	41.8	1709	14.2	40.9
SIPN-8-2-10	8:2:10	151.6	45.9	2178	14.4	47.5
SIPN-7-3-10	7:3:10	203.5	65.4	2980	14.7	45.7
SIPN-5-5-10	5:5:10	167.5	47.2	2463	14.7	52.1
SIPN-3-7-10	3:7:10	151.6	38.5	2365	15.6	61.4
SIPN-0-10-10	0:10:10	122.1	26.8	1767	14.5	65.9

Table. S5. Gas permeability and selectivity of SIPN-7-3-Z membranes

Membrane	PEGMEA:PEGDA:PEGDME	Permeability (Barrer)			Ideal Selectivity	
		H ₂	N ₂	CO ₂	CO ₂ /H ₂	CO ₂ /N ₂
SIPN-7-3-0	7:3:0	39.9	8.2	405.7	10.2	49.8
SIPN-7-3-3	7:3:3	116.3	30.2	1409	12.1	46.7
SIPN-7-3-5	7:3:5	156.8	44.5	2095	13.4	47.1
SIPN-7-3-7	7:3:7	171.4	52.3	2461	14.4	47.1
SIPN-7-3-10	7:3:10	203.5	65.4	2980	14.7	45.7

Table. S6 CO₂ diffusivity, solubility and selectivity over N₂ for SIPN-X-Y-10

Membrane	CO ₂		N ₂		CO ₂ /N ₂	
	D	S	D	S	α_D	α_S
SIPN-0-10-10	5.24	3.33	3.20	0.0838	1.64	39.8
SIPN-3-7-10	6.39	3.64	3.87	0.0876	1.45	41.5
SIPN-5-5-10	6.50	3.70	3.98	0.0916	1.27	40.4
SIPN-7-3-10	7.72	3.84	4.50	0.0927	1.10	41.4
SIPN-8-2-10	6.69	3.25	5.05	0.0854	1.25	38.0
SIPN-9-1-10	6.09	2.81	5.09	0.0821	1.20	34.2

D×10⁶ cm²/s and S×10² cm³/cm³ cm Hg

Table. S7 CO₂ diffusivity, solubility and selectivity over N₂ for SIPN-7-3-Z.

Membrane	CO ₂		N ₂		CO ₂ /N ₂	
	D	S	D	S	α_D	α_S
SIPN-7-3-0	1.66	2.45	1.27	0.0640	1.30	38.3
SIPN-7-3-3	4.36	3.23	2.72	0.109	1.60	29.7
SIPN-7-3-5	5.34	3.89	3.37	0.132	1.58	29.4
SIPN-7-3-7	5.98	3.81	3.44	0.152	1.74	25.0
SIPN-7-3-10	7.72	3.84	4.02	0.163	1.92	23.6

D×10⁶ cm²/s and S×10² cm³/cm³ cm Hg

Reference

- 1 Y. Liu, R. Wang and T.-S. Chung, *J. Membrane Sci.*, 2001., 189, 231-239.
- 2 A. Strzelewicz and Z. J. Grzywna, *J. Membr. Sci.*, 2008, 322, 460-465.
- 3 J. Xia, T.-S. Chung and D. R. Paul, *J. Membr. Sci.*, 2014, 450, 457-468
- 4 P. S. Tin, T. S. Chung, Y. Liu, R. Wang, S. L. Liu and K. P. Pramoda, *J. Membr. Sci.*, 2003, 225, 77-90.
- 5 S. Wan, C. Waters, A. Stevens, A. Gumidyala, R. Jentoft, L. Lobban, D. Resasco, R. Mallinson and S. Crossley, *ChemSusChem*, 2015, 8, 552-559.
- 6 N. L. Le, Y. P. Tang and T.-S. Chung, *J. Membrane Sci.*, 2013, 447, 163-176.
- 7 Y. C. Jean, Q. Deng and T. T. Nguyen, *Macromolecules*, 1995, 28, 8840-8844.
- 8 Y. C. Jean, J. P. Yuan, J. Liu, Q. Deng and H. Yang, *J. Polym. Sci. Polym. Phys.*, 1995, 33, 2365-2371.
- 9 Y.-J. Fu, J.-T. Chen, C.-C. Chen, K.-S. Liao, C.-C. Hu, K.-R. Lee and J.-Y. Lai, *Polym. Eng. Sci.*, 2013, 53, 1623-1630.